A comparative study of the biological effects of various mobile phone and wireless LAN antennas

ARTICLE *in* IEEE TRANSACTIONS ON MAGNETICS · APRIL 2002

Impact Factor: 1.21 · DOI: 10.1109/20.996201 · Source: IEEE Xplore

7 AUTHORS, INCLUDING:

Theodoros Kosmanis
Alexander Technological Educational Institut…
26 PUBLICATIONS **82** CITATIONS
SEE PROFILE

Theodoros T. Zygiridis
University of Western Macedonia
42 PUBLICATIONS **160** CITATIONS
SEE PROFILE

A Comparative Study of the Biological Effects of Various Mobile Phone and Wireless LAN Antennas

T. V. Yioultsis, T. I. Kosmanis, E. P. Kosmidou, T. T. Zygiridis, N. V. Kantartzis, T. D. Xenos, and T. D. Tsiboukis

***Abstract*—This paper presents a comprehensive electromagnetic and thermal analysis of radiation and its impact on human beings, due to the use of various types of commonly used mobile phones and communication antennas. This is one of the first studies that deals with a wide-range comparative investigation of modern cell phones, unlike the majority of existing work, which do not extend beyond the obsolete generic phone case. The rather severe, although overlooked, case of wireless local area network antennas is also considered, due to their increasing use and the large times of exposure associated with them.**

***Index Terms*—Biological application of electromagnetic radiation, electromagnetic radiation effects, FDTD methods, mobile antennas.**

I. Introduction

THE INVESTIGATION of the effects of nonionizing electromagnetic radiation is considered a principal area of research in bioelectromagnetics. Of particular interest is the study of certain wireless systems, such as the cell phones and wireless local area network (WLAN) antennas, due to their increasing importance and widespread use in modern communication systems. At the same time, the significant development of numerical methods for electromagnetic field computation along with the progress in computer technology has provided a set of rigorous tools for electromagnetic field computation. Several studies concerning the interaction of cell phones or other portable antennas can be found in the literature [1]–[5].

However, the majority of computational investigations deal with simplified, generic phone models. In particular, only the standard cases of half-wavelength dipoles in free space or quarter-wavelength monopoles mounted on a metallic box are usually considered, which correspond to a cell phone configuration that is no longer in widespread use. On the other hand, modern types of phones have been designed, mostly motivated by the need for size reduction and design improvement, using alternative kinds of antennas such as helical, microstrip, or other patch antennas. Hence, there is a question of whether contemporary cell phone design meets the need for protection against electromagnetic radiation, without a significant decrease in efficiency. Moreover, the use of certain antenna types like the WLAN establishes conditions of long-term exposure which, apart from the adverse thermal consequences, raise the issue of the investigation of possible nonthermal effects and requires compliance with safety standards against chronic exposure [6].

This is one of the first studies to attempt a large-scale comparative investigation of the radiation characteristics of several phone antennas with emphasis on modern cell phones using monopole, helical, side-mounted planar inverted-F antenna (PIFA) and patch antennas. The electromagnetic analysis is enhanced by subgridding techniques, which provide enhanced accuracy in modeling thin geometric structures [7], while a thermal model, including an efficient discretization technique, is used to investigate the thermal effects of radiation. The whole study reveals the occurrence of considerable differences in electric field or specific absorption rate (SAR) values. The most striking result is the high absorption from the head, which, apart from its possible biological influence, results in remarkable degradation of the antenna efficiency. This observation could be exploited in the design of phone antennas to avoid the main bulk of useless radiation toward the direction of human body.

II. Computational FDTD Models

A detailed three–dimensional (3-D) computational model of the human head has been used in the calculations, which are conducted by means of an FDTD algorithm [8] with the appropriate choice of dielectric properties [2], [4], [5]. The excitation used in the calculations has the general form of a sinusoidal waveform

$$E_i = E_0 \left(1 - e^{-(t/T_0)}\right) \sin(2\pi f t) \tag{1}$$

where a suitable exponential term has been added in the simulation to reduce numerical dispersion. A Berenger perfectly matched layer (PML) has been applied to efficiently terminate the computational domain. The use of an eight-layer PML has enabled the reduction of the computational domain to a $101 \times 107 \times 109$ grid, resulting in computational times of the order of a few hours.

Due to the complexity of the structures considered, we have further enhanced our computational model by means of an appropriate subgridding technique, when thin geometries like wires, helices and thin patches had to be modeled. In particular, the subgrid is placed within the coarse grid (Fig. 1) such that its boundaries are as close as possible but not coinciding to the boundaries of the dual coarse grid. Apart from the standard FDTD update schemes in both grids, all components of the fine

Manuscript received July 2, 2001. This work was supported in part by the Greek General Secretariat of Research and Technology under Grant ED325/PENED 99 and in part by the Municipality of Serres under Grant RC-AUTH/20179.

The authors are with the Department of Electrical and Computer Enginnering, Division of Telecommunications, Aristotle University of Thessaloniki, GR-54006, Greece (e-mail: tsibukis@eng.auth.gr).

Publisher Item Identifier S 0018-9464(02)01584-4.

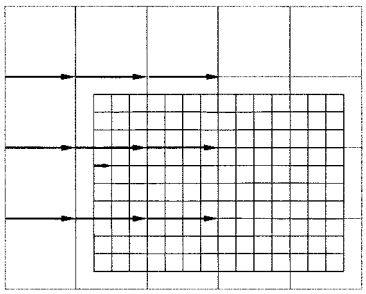

Fig. 1. Placement of subgrid with respect to the coarse grid. Any component in the transition region (short arrow) is updated using three components from the coarse grid in each direction (long arrows).

grid which are in the transition region and cannot be updated are expressed in terms of an efficient spline-approximation scheme via least squares, using three components from the coarse grid in each direction. On the other hand, coarse-grid components that are overlapped by fine-grid ones are simply interpolated. Finally, for missing temporal components, simple extrapolation techniques are incorporated. The entire algorithm is stable and the memory requirements are not significantly increased, whereas the computational time may be two times the initial one or more, due to the smaller time step in the subgrid, and also depending on the subgrid's size and ratio.

Several cell phone antennas have been considered in this study. The first generic model is the quarter wavelength dipole, mounted on a conducting box. This assumption is justified by the presence of the printed circuit board and battery but it is appropriately modified for other types of phones to result in a more accurate modeling. The second model is based on the more common helical antenna. Such antennas, for small values of their diameter and length, result in nearly isotropic radiation on the horizontal plane. The third and fourth models correspond to modern types of phones using patch antennas. This may enhance the phone's look, but requires very careful design to produce the desirable radiation pattern. The side-mounted PIFA and another patch antenna model (Fig. 2) are among the most common to be used. The computation procedure results in the values of antenna efficiency and SAR, given by

$$\alpha = \left(P_{\text{in}} - \int_{\text{head}} \sigma |E|^2 \, dv \right) / P_{\text{in}} \tag{2}$$

$$\text{SAR} = \frac{\sigma |E|^2}{2\rho}. \tag{3}$$

The SAR values are postprocessed to produce average quantities involved in safety standards.

III. Thermal Analysis

The electromagnetic analysis gives only a rough picture of how the power is absorbed by the tissues. However, this cannot account for the exact description of thermal phenomena, since they are significantly affected by the material parameters [4], [5] and the existence of discontinuities. Therefore, we pursue an investigation of the thermal effects, by means of the bioheat equation [2], [4], [5]

$$K \cdot \nabla^2 T + A_0 + \rho \cdot \text{SAR} - B \cdot (T - T_b) = C \cdot \rho \cdot \frac{\partial T}{\partial t}. \tag{4}$$

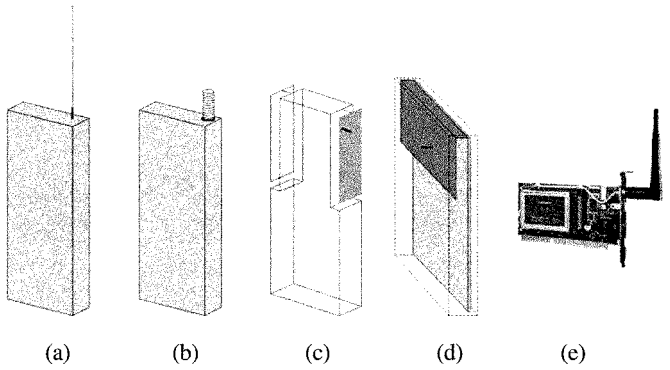

Fig. 2. Mobile phone and WLAN antennas under consideration. (a) Quarter wavelength monopole. (b) Helix. (c) Side-mounted PIFA. (d) Patch. (e) WLAN antenna. Feeds are shown with a thick line.

where

- T temperature distribution;
- K thermal conductivity;
- C specific heat;
- ρ density;
- A_0 power per unit volume, generated by metabolism;
- T_b blood temperature;
- B constant related to blood flow.

Of great importance is the boundary condition to be imposed to the external surface of the skin and internal cavity, given by

$$-K \frac{\partial T}{\partial t}\bigg|_S = h(T - T_a) \tag{5}$$

where h is the convective heat-transfer coefficient and T_a the ambient temperature. This condition accounts for the heat-exchange mechanism of convection from the surrounding medium.

However, we introduce a slightly modified approach in this study which focuses on the thermal rise only, due to power absorption, while other factors that contribute to the overall thermal equilibrium are properly removed from the analysis. Hence, if we consider the resulting temperature distribution T as the sum of the thermal equilibrium distribution T_o and the temperature rise ΔT, the corresponding equations for the equilibrium temperature distribution are similar to (4) and (5), except that the SAR-related term is not present. Taking this into account, the bio-heat equation and convective boundary condition for the temperature rise are, respectively, given by

$$K \cdot \nabla^2 \Delta T + \rho \cdot \text{SAR} - B \cdot \Delta T = C \cdot \rho \cdot \frac{\partial \Delta T}{\partial t} \tag{6}$$

$$-K \frac{\partial \Delta T}{\partial t}\bigg|_S = h \Delta T. \tag{7}$$

Therefore, the power due to metabolism, and the blood and ambient temperatures, do not affect the temperature rise.

The thermal diffusion equation (6) can be discretized by means of an Euler conditionally stable finite-difference scheme using central differences for the Laplacian and forward differences for the time derivative, on condition that the maximum

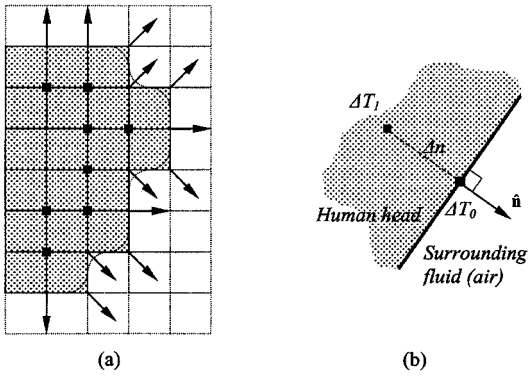

Fig. 3. Quasiconformal representation of: (a) the exterior head and internal cavity surface and (b) the discretization scheme for the convective heat-transfer boundary condition.

allowable time step is not prohibitive for an efficient impementation. The discretized form of (6) is therefore

$$\Delta T_{i,j,k}^{n+1} = \left(1 - \frac{B_{i,j,k}\Delta t}{C_{i,j,k}\rho_{i,j,k}} - \frac{6K_{i,j,k}\Delta t}{C_{i,j,k}\rho_{i,j,k}\Delta^2}\right)\Delta T_{i,j,k}^{n} + \frac{K_{i,j,k}\Delta t}{C_{i,j,k}\rho_{i,j,k}\Delta^2} \cdot \begin{pmatrix} \Delta T_{i+1,j,k}^{n} + \Delta T_{i,j+1,k}^{n} \\ +\Delta T_{i,j,k+1}^{n} + \Delta T_{i-1,j,k}^{n} \\ +\Delta T_{i,j-1,k}^{n} + \Delta T_{i,j,k-1}^{n} - 6\Delta T_{i,j,k}^{n} \end{pmatrix} + \frac{\Delta t}{C_{i,j,k}}\,\mathrm{SAR}_{i,j,k}. \quad (8)$$

Using the von Neumann stability criterion, we have verified that the stability condition is

$$\Delta t \leq \frac{2C\rho\Delta^2}{12K + B\Delta^2} \cong \frac{C\rho\Delta^2}{6K} \quad (9)$$

which, for a cell size of 3 mm, gives a maximum allowable time step of 5.83 s, resulting in less than 500 iterations, even for a 30-min duration of radiation.

On the other hand, the convective condition requires an elaborate discretization scheme to be efficiently implemented. While in [2] and [4] this boundary condition is applied in a rather simplified manner, we introduce a *quasiconformal* representation of the exterior surface [Fig. 3(a)]. The normal vector follows the shape of the head and is oriented toward either the x, y, or z axis, or some of the possible diagonal xy, yz, zx, or xyz directions. In general, the discretized form of (7) will update the temperature value at any surface node ΔT_0 using the corresponding value at the adjacent node ΔT_l [Fig. 3(b)]. Therefore, (7) results in

$$\Delta T_0^{n+1} = \frac{K\Delta T_1^{n+1}}{K + h\Delta n}. \quad (10)$$

Hence, while the interior diffusion scheme is used to update all values inside the tissues, including those at nodes adjacent to the surface, the discrete form (7) of the convective heat-transfer boundary condition updates the surface node values and the algorithm proceeds with the next time step. Although simple in application, (7) requires a geometric preprocessing procedure to associate each one of the surface nodes to an interior one toward the direction of the inward pointing normal vector [Fig. 3(a)]. The overall algorithm involves about 500 000 nodal degrees of freedom and requires only a few minutes to result in the steady-state thermal rise distribution.

TABLE I
MAXIMUM SAR QUANTITIES (W/kg) AND EFFICIENCY FOR VARIOUS ANTENNA TYPES (GSM 900)

		Max SAR	Max 1g Avg SAR	Max 10 g Avg SAR	Antenna Efficiency
Monopole	V	7.993	3.181	2.061	25.29 %
	T	4.596	2.925	2.072	30.40 %
Helix	V	7.255	4.011	2.531	54.36 %
	T	5.771	3.477	2.385	62.21 %
Side PIFA	V	13.852	5.305	3.299	20.41 %
	T	6.078	3.902	2.430	29.57 %
Patch antenna	V	7.819	4.76412	3.178	28.50 %
	T	8.622	5.02242	3.105	31.37 %

TABLE II
MAXIMUM SAR QUANTITIES (W/kg) AND EFFICIENCY FOR VARIOUS ANTENNA TYPES (GSM 1800, WLAN)

		Max SAR	Max 1g Avg SAR	Max 10 g Avg SAR	Antenna Efficiency
Monopole	V	2.171	1.473	0.946	64.98 %
	T	2.013	1.141	0.689	64.80 %
Helix	V	3.838	8.550	5.402	46.07 %
	T	3.347	6.621	4.097	53.21 %
Side PIFA	V	16.032	8.769	4.565	23.78 %
	T	8.372	5.397	3.302	33.43 %
Patch antenna	V	1.152	0.855	0.591	66.33 %
	T	0.808	0.626	0.447	71.82 %
WLAN	-	0.231	0.089	0.064	-

TABLE III
MAXIMUM TEMPERATURE RISE IN HUMAN HEAD (°C) AND BRAIN

		Max ΔT (900)	Max ΔT (1800)	Max ΔT in brain (900)	Max ΔT in brain (1800)
Monopole	V	0.355	0.158	0.177	0.0302
	T	0.562	0.102	0.331	0.0389
Helix	V	0.381	0.089	0.169	0.045
	T	0.369	0.061	0.178	0.033
Side PIFA	V	0.551	0.712	0.158	0.063
	T	0.416	0.571	0.139	0.058
Patch antenna	V	0.541	0.109	0.240	0.079
	T	0.569	0.072	0.380	0.016
WLAN	-	5.011e-5		1.982e-5	

IV. COMPUTATIONAL RESULTS

A large number of numerical simulations has been conducted for the GSM 900 and 1800 case, with an input power of 600 and 250 mW, respectively. Both the vertical (V) and tilted (T) positions of the phones have been examined. The WLAN antenna has an input power of +20 dBm at the frequency of 2.45 GHz. The comparative results for the maximum SAR, and maximum 1- and 10-g average SAR quantities, are given in Tables I and II, while Table III shows the overall maximum and maximum in brain temperature rise for 10-min exposure. Indicative SAR and thermal rise distribution maps are also shown for the case of a tilted PIFA antenna at 900 MHz (Figs. 4 and 5), a tilted patch antenna at 1800 MHz (Figs. 6 and 7), and a WLAN antenna (Fig. 8). We use a rather unusual notation of decibels with respect to 1 °C for the temperature rise distribution, but this is

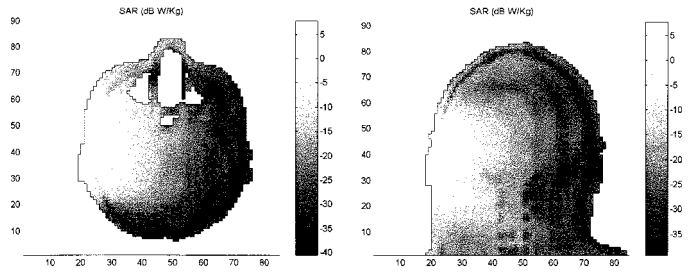

(a) (b)

Fig. 4. SAR images in decibels (W/kg) in the (a) coronal and (b) frontal section of the human head for a tilted PIFA antenna phone at 900 MHz.

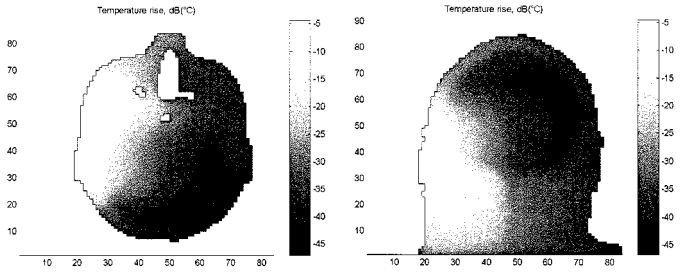

(a) (b)

Fig. 5. Thermal rise distribution in decibels (1 °C) in the (a) coronal and (b) frontal section of the human head for a tilted PIFA antenna phone at 900 MHz.

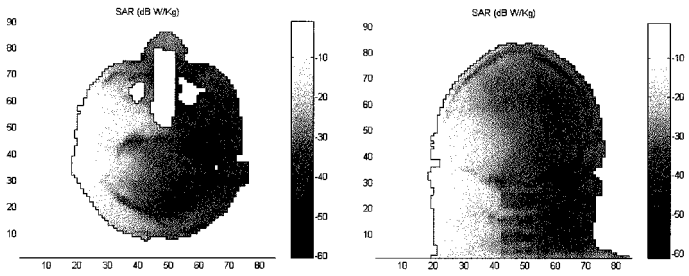

(a) (b)

Fig. 6. SAR images in decibels (W/kg) in the (a) coronal and (b) frontal section of the human head for a tilted patch antenna phone at 1800 MHz.

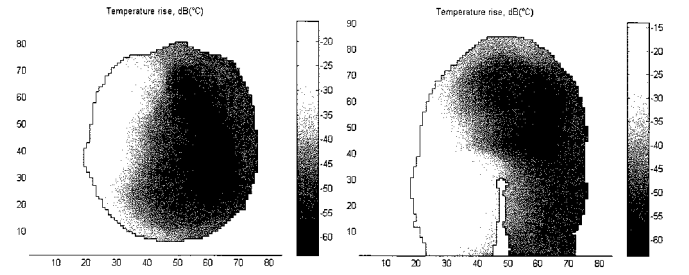

(a) (b)

Fig. 7. Thermal rise distribution in decibels (1 °C) in the (a) coronal and (b) frontal section of the human head for a tilted patch antenna phone at 1800 MHz.

justified by the fact that the latter one is linearly related to SAR values.

In most cases, the derived SAR values are found to violate the safety guidelines of 1.6 W/kg maximum, 1-g average [9], and 2.0-W/kg maximum, 10-g average [10] marginally, but the time of exposure is relatively short to produce remarkable thermal effects. However, we observe a considerable reduction of thermal effect in the 1800-MHz case, where patch-based antennas also

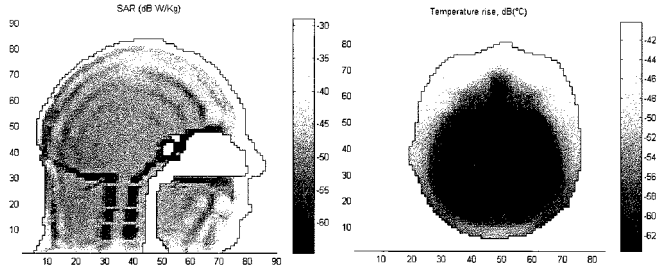

Fig. 8. SAR image in a saggital and temperature rise distribution in a coronal section of the human head for the WLAN case at 2.45 GHz.

exhibit a good performance. On the other hand, although both SAR values and the thermal rise in the case of a WLAN are one or two orders of magnitude lower, the issue of prolonged exposure is raised, since it is found that the safety limits for long exposure [6] are also marginally violated.

V. Conclusion

A systematic investigation of electromagnetic radiation due to a variety of modern cell phone and wireless network antennas, and its effects on human health has been presented. The computational analysis, based on the FDTD method, and an efficient thermal analysis demonstrate significant differences both in local and average SAR values or electric fields and radiation characteristics, which is a sign of different degrees of interaction between the antenna and the human head. Hence, useful antenna design guidelines, such as the use of appropriate reflecting surfaces, may be exploited. In cases where suggested time limits of exposure are exceeded, and especially in the case of WLANs, the possibility of harmful thermal or nonthermal influences of radiation should not be ruled out and is a matter of further investigation.

References

[1] G. Lazzi, S. S. Pattnaik, C. M. Furse, and O. P. Gandhi, "Comparison of FDTD computed and measured radiation patterns of commercial mobile telephones in presence of the human head," *IEEE Trans. Antennas Propagat.*, vol. 46, pp. 943–944, June 1998.

[2] P. Bernardi, M. Cavagnaro, S. Pisa, and E. Piuzzi, "SAR distribution and temperature increase in an anatomical model of the human eye exposed to the field radiated by the user antenna in a wireless LAN," *IEEE Trans. Microwave Theory Tech.*, vol. 46, pp. 2074–2082, Dec. 1998.

[3] K. Meier, V. Hombach, R. Kästle, R. Y.-S. Tay, and N. Kuster, "The dependence of electromagnetic energy absorption upon human-head modeling at 1800 MHz," *IEEE Trans. Microwave Theory Tech.*, vol. 45, pp. 2058–2062, Nov. 1997.

[4] J. Wang and O. Fujiwara, "FDTD computation of temperature rise in the human head for portable telephones," *IEEE Trans. Microwave Theory Tech.*, vol. 47, pp. 1528–1534, Aug. 1999.

[5] P. Bernardi, M. Cavagnaro, S. Pisa, and E. Piuzzi, "Specific absorption rate and temperature increases in the head of a cellular-phone user," *IEEE Trans. Microwave Theory Tech.*, vol. 48, pp. 1118–1126, July 2000.

[6] P. Czerski, "Radiofrequency radiation exposure limits in Eastern Europe," *J. Microw. Power*, vol. 21, no. 1, pp. 9–23, 1986.

[7] M. Okoniewski, E. Okoniewska, and M. Stuchly, "Three-dimensional subgridding algorithm for FDTD," *IEEE Trans. Antennas Propagat.*, vol. 45, pp. 422–429, March 1997.

[8] A. Taflove, Ed., *Advances in Computational Electrodynamics: The Finite-Difference Time-Domain Method*. Norwood, MA: Artech, 1998.

[9] *IEEE Standard for Safety Levels with Respect to Human Exposure to RF Electromagnetic Fields*, IEEE C95.1, IEEE, New York, 1995.

[10] "Human exposure to electromagnetic fields: High frequency (10 KHz to 300 GHz)," CENELEC, ENV 50 166-2, 1995.